Enhancing high-order harmonic generation by sculpting waveforms with chirp

Dian Peng (彭典),[1] M. V. Frolov,[2] Liang-Wen Pi (皮良文),[3] and Anthony F. Starace[1]
[1]*Department of Physics and Astronomy, University of Nebraska, Lincoln, Nebraska 68588-0299, USA*
[2]*Department of Physics, Voronezh State University, Voronezh 394018, Russia*
[3]*Max-Planck-Institut für Physik komplexer Systeme, D-01187 Dresden, Germany*

(Received 3 February 2018; published 29 May 2018)

We present a theoretical analysis showing how chirp can be used to sculpt two-color driving laser field waveforms in order to enhance high-order harmonic generation (HHG) and/or extend HHG cutoff energies. Specifically, we consider driving laser field waveforms composed of two ultrashort pulses having different carrier frequencies in each of which a linear chirp is introduced. Two pairs of carrier frequencies of the component pulses are considered: (ω, 2ω) and (ω, 3ω). Our results show how changing the signs of the chirps in each of the two component pulses leads to drastic changes in the HHG spectra. Our theoretical analysis is based on numerical solutions of the time-dependent Schrödinger equation and on a semiclassical analytical approach that affords a clear physical interpretation of how our optimized waveforms lead to enhanced HHG spectra.

DOI: 10.1103/PhysRevA.97.053414

I. INTRODUCTION

The electric-field waveform of a laser pulse plays a crucial role in high-order harmonic generation (HHG) by a few-cycle driving laser field [1]. Specifically, HHG spectra can be very sensitive to the carrier-envelope phase (CEP) [2] and the chirp [3,4] of a single few-cycle pulse, or to the time delay between two-color synthesized few-cycle laser pulses [5]. An optimized few-cycle or many-cycle waveform of the laser field can, e.g., selectively enhance a single harmonic while suppressing neighboring harmonics [6–8], or, alternatively, greatly enhance HHG yields across a large range of harmonic photon energies [5,9–16].

Waveform control in HHG is typically realized by coherently combining two or more color laser pulses while carefully adjusting the phases, intensities, and, in some cases, the polarizations of the component frequencies [7,11,12,15–17]. The values of the parameters are often obtained by optimization techniques using iterative algorithms with feedback loops [6,8,9,11–16], but can also be determined on the basis of physical arguments, e.g., for the purpose of increasing ionization rates and/or recollision energies of the active electron in HHG processes [5,9,10]. Chirp is an additional parameter for controlling the driving laser waveform and, hence, HHG spectra. The value of the chirp parameter in a linearly chirped *many-cycle* driving laser pulse has been shown to greatly affect the shape of the HHG spectrum because it can compensate the chirp of the emitted harmonics [18–21]. More recently, the use of waveforms composed of two or more color, linearly chirped many-cycle driving laser pulses has been shown to enable one to selectively enhance particular harmonics [7,8].

In this paper, we study HHG spectra produced by two-color, *few-cycle* linearly chirped laser pulse fields. We show how the chirps of the two-color pulses can be used to synthesize few-cycle waveforms that result in enhanced HHG yields and/or extended HHG cutoff energies. Results are presented for two common cases of two-color waveforms, i.e., those formed from ω–2ω and ω–3ω few-cycle pulses. Our results are obtained by solving the time-dependent Schrödinger equation (TDSE) as well as by means of a closed-form analytic quantum description of HHG spectra produced by few-cycle pulses [22]. The latter analytic theory enables us to interpret our results in terms of the key trajectories of the active electron, thus making a straightforward connection to the semiclassical three-step model of HHG [1,23–26].

This paper is organized as follows. In Sec. II we present our theoretical formulation, including a description of our parametrization of two-color chirped few-cycle pulses and a brief overview of our numerical and analytic methods for calculating HHG spectra. In Sec. III we present our numerical and analytic results for HHG spectra produced by the important cases of ω–2ω and ω–3ω few-cycle, chirped laser pulse waveforms. For each case we discuss our strategy for using the chirp of each of the two few-cycle pulses to enhance the HHG yield and/or to extend the HHG cutoff energy. Finally, in Sec. IV we summarize our results on using two-color, chirped few-cycle pulse waveforms to enhance HHG yields and cutoff energies and present some conclusions. Atomic units (a.u.) are used throughout this paper unless otherwise specified.

II. THEORETICAL FORMULATION

In this section we present general descriptions of our theoretical formulation. Specifically, we first discuss how we parametrize chirped pulses and then provide brief descriptions of the two methods we employ to calculate HHG spectra. Details of our pulse parameters are given in Sec. III, where we present our HHG results.

A. Description of a short laser-field pulse

In the electric dipole approximation, the spatial dependence of a laser field is neglected and in order to avoid any zero-frequency component the electric field $\mathbf{F}(t)$ of a laser pulse is

 ©2018 American Physical Society

calculated from the vector potential, $\mathbf{A}(t)$:

$$\mathbf{F}(t) = -\frac{1}{c}\frac{\partial \mathbf{A}(t)}{\partial t}, \tag{1}$$

where c is the speed of light. A general parametrization of the vector potential for a linearly polarized field is

$$\mathbf{A}(t) = -\frac{cF}{\omega} f(t)\sin[\phi(t)]\hat{\mathbf{z}}, \tag{2}$$

where F is the peak strength, ω is the carrier frequency, $f(t)$ is the temporal envelope of the laser pulse, and $\phi(t)$ is a phase function. For a chirp-free pulse, the phase function is a linear function of time, $\phi(t) = \phi_0 + \omega t$, where ϕ_0 is the CEP.

B. Description of chirped pulses

There are two commonly used analytic descriptions of a linearly chirped laser pulse. One way is to simply add a term in the chirp-free phase function that is quadratic in the time t so that the laser field has a time-dependent frequency that is linear in time, as done in Refs. [4,8,18]. In order to determine the role of the chirp, typically the pulse durations and peak amplitudes are fixed (i.e., independent of chirp). For an ultrashort laser pulse, which has a frequency bandwidth, a different description has been used in which the frequency bandwidth of the chirped pulse is kept the same as that of the corresponding chirp-free pulse [27,28]. In this paper we combine aspects of both pulse formulations.

Specifically, the phase function $\phi(t)$ for a linearly chirped pulse has the form

$$\phi(t) = \phi_0 + \omega t + \frac{\delta}{2}t^2, \tag{3}$$

where $\delta = d^2\phi(t)/dt^2$ is the pulse chirp. In this paper the vector potential (2) for each of the two linearly chirped components i of a two-color laser pulse waveform [with each component having a Gaussian-shaped temporal envelope $f_i(t) \equiv e^{-\alpha_i t^2}$] thus takes the form

$$\mathbf{A}_i(t) = -\frac{cF_i}{\omega_i} e^{-\alpha_i t^2}\sin(\omega_i t + \delta_i t^2/2 + \phi_i), \tag{4}$$

where F_i, ω_i, ϕ_i, and δ_i are the amplitude, frequency, CEP, and chirp parameter of the ith color field. The Gaussian envelope parameter α_i is related to the pulse duration τ_i by $\alpha_i = 2\ln 2/\tau_i^2$, where the pulse duration τ_i is defined as the full width at half maximum of the intensity profile. It is convenient to introduce a dimensionless chirp parameter β_i, defined by

$$\delta_i = 2\alpha_i\beta_i. \tag{5}$$

Then the pulse duration τ_i may be expressed as

$$\tau_i^2 = \Delta_i^2\left(1+\beta_i^2\right), \tag{6}$$

where Δ_i is the pulse duration in the absence of chirp, i.e., when $\beta_i = 0$. The chirp-independent bandwidth Γ_i of the ith component pulse is then

$$\Gamma_i = 4\ln 2/\Delta_i. \tag{7}$$

In this paper we consider two-color pulse waveforms in which $i = 1$ corresponds to the component pulse with a carrier frequency ω, $i = 2$ corresponds to one with carrier frequency 2ω, and $i = 3$ corresponds to one with carrier frequency 3ω. The vector potential for the two-color pulse waveform for the ω–2ω case is thus

$$\mathbf{A_{1+2}}(t) = \mathbf{A}_1(t) + \mathbf{A}_2(t), \tag{8}$$

and the one for the ω–3ω case is

$$\mathbf{A_{1+3}}(t) = \mathbf{A}_1(t) + \mathbf{A}_3(t). \tag{9}$$

Note that the durations of these three component pulses are assumed to be different, since in experiments these can be separately adjusted (see, e.g., Refs. [29–31]). Specifically, we assume that the parameter Δ_i equals

$$\Delta_i = \sqrt{i}\,T_i\,, \tag{10}$$

where the period T_i is defined by $T_i \equiv 2\pi/\omega_i$. For clarity in this paper, we focus only on the sign of the chirp, i.e., we compare results for positive ($\beta_i > 0$) and negative ($\beta_i < 0$) chirps having the same absolute magnitude, which is fixed at $|\beta_i| = 2$ in all calculations with chirped pulses. Thus our chirped pulses have pulse durations

$$\tau_i = \sqrt{5}\Delta_i = \sqrt{5i}\,T_i. \tag{11}$$

With two colors and the choice of positive (+) or negative (−) chirp for each color, there are four possible combinations of chirp, i.e., (+,+), (+,−), (−,+), and (−,−).

Our goal is to determine which combinations give the highest HHG yields and cutoff energies. Since our aim is to focus on the role of chirp in optimizing the short-pulse waveform, when comparing results for our two-color chirped pulses to results for two-color unchirped pulses, we keep the pulse durations τ_i for both chirped and unchirped pulses the same. As we shall show, for few-cycle pulses the most important features of the two-color pulse waveform are those in the neighborhood of the peaks of the two-color pulse envelopes and thus the results we present are not very sensitive to the differences in the pulse durations of the ω pulse (τ_1) and the 2ω pulse (τ_2) or 3ω pulse (τ_3).

C. Calculation of HHG spectra

The HHG spectra are calculated using the two methods used in Ref. [5]. One is to solve the three-dimensional TDSE for an H atom interacting with a laser electric field $F(t)$ that is linearly polarized along the z axis. Within the dipole approximation, the azimuthally symmetric TDSE is thus

$$i\frac{\partial}{\partial t}\Psi(\boldsymbol{r},t) = \left[\frac{\boldsymbol{p}^2}{2} - \frac{1}{r} + zF(t)\right]\Psi(\boldsymbol{r},t), \tag{12}$$

where the electric field $F(t)$ is derived from the vector potential in either Eq. (8) or (9): $F(t) = -\partial_t A(t)/c$, in which $A(t) \equiv \mathbf{A}(t)\cdot\hat{\mathbf{z}}$. The TDSE is solved in spherical coordinates using a time-dependent generalized pseudospectral method [32], in which the wave function is expanded in Legendre polynomials and the time propagation is carried out using a second-order split-operator technique. The convergence of our TDSE calculations was monitored by increasing the basis size and the grid density in both space and time.

The dimensionless harmonic spectrum $S(\Omega)$ is obtained from the Fourier transformed dipole acceleration along the z axis $\ddot{D}_z(\Omega)$:

$$S(\Omega) = \frac{1}{\hbar c^3}|\ddot{D}_z(\Omega)|^2, \tag{13}$$

where the Fourier transform is defined by

$$\ddot{D}_z(\Omega) = \frac{1}{\sqrt{2\pi}}\int_{-\infty}^{\infty}\ddot{D}_z(t)e^{-i\Omega t}dt\,, \tag{14}$$

and the time-dependent dipole acceleration $\ddot{D}_z(t)$ is [33]

$$\begin{aligned}\ddot{D}_z(t) &\equiv \langle\Psi(\boldsymbol{r},t)| - \ddot{z}|\Psi(\boldsymbol{r},t)\rangle \\ &= \langle\Psi(\boldsymbol{r},t)|\frac{\partial V(r)}{\partial z}|\Psi(\boldsymbol{r},t)\rangle + F(t)\,,\end{aligned} \tag{15}$$

in which $V(r) = -1/r$ is the atomic potential for an H atom, and thus $\partial V(r)/\partial z = z/r^3$. Note that the factor $\hbar c^3$ in the denominator of Eq. (13) has been given explicitly (where $\hbar = 1$ in a.u.) in order to clearly indicate that $S(\Omega)$ is dimensionless.

The second method employs an analytical description of HHG spectra produced by few-cycle laser pulses [22]. In this analytic description, the dimensionless harmonic spectrum $\rho(\Omega)$ is obtained by coherently adding a handful of amplitudes corresponding to ionized electron trajectories (labeled by j and k) from different half cycles of the laser pulse:

$$\rho(\Omega) = \sum_{j,k} s_{jk}\cos(\varphi_j - \varphi_k)\mathcal{A}_j(E)\mathcal{A}_k(E), \tag{16}$$

where the harmonic photon energy Ω and the returning electron energy E satisfy the relation

$$\Omega = E + |E_0|. \tag{17}$$

Here E_0 is the ground-state energy of the electron, which equals $E_0 = -1/2$ for the hydrogen atom. In Eq. (16), each amplitude $\mathcal{A}_j(E)$ equals the square root of a product of three factors representing the three steps of high harmonic generation: the ionization factor $\mathcal{I}_j$, the propagation factor $\mathcal{W}_j(E)$, and the recombination factor $\sigma^{(r)}(E)$:

$$\mathcal{A}_j(E) \equiv \sqrt{\mathcal{I}_j\mathcal{W}_j(E)\sigma^{(r)}(E)}\,. \tag{18}$$

Also, in Eq. (16) φ_j is the phase of the jth amplitude and the factors $s_{jk} = \pm 1$ are sign factors. The calculation of each $\mathcal{A}_j(E)$ amplitude begins by finding a corresponding classical trajectory that starts at $t_i^{(j)}$ (the ionization time), and ends at $t_r^{(j)}$ (the recombination time). For a detailed description of the calculation of the amplitudes $\mathcal{A}_j(E)$, the phases φ_j, the sign factors s_{jk}, and the times $t_i^{(j)}$ and $t_r^{(j)}$, see Refs. [5,22].

III. RESULTS AND DISCUSSION

Commonly used two-color fields include those in which a pulse with carrier frequency ω is combined with either a second-harmonic pulse ($\omega - 2\omega$) or a third-harmonic pulse ($\omega - 3\omega$). These two combinations can have very different alignments of the fundamental and harmonic field maxima and minima. For the $\omega - 2\omega$ field waveform one can never align all the major extrema of the two color constituents. As shown in Fig. 1(a), the maxima are aligned at $t = 0$ but are antialigned at $t = 0.5T_1$, where T_1 is the period of the fundamental frequency. However, for the $\omega - 3\omega$ field waveform, the extrema can be aligned at both $t = 0$ and $0.5T_1$ [see Fig. 3(a) below]. Owing to such different alignment possibilities as well as to the fact that HHG spectra are extremely sensitive to the time profile of a laser pulse waveform, the strategies for choosing the best chirp combinations are different for the $\omega - 2\omega$ and $\omega - 3\omega$ field waveforms. These different strategies are discussed in turn in Secs. III A and III B for pulses having zero CEPs (so that the two fields are aligned at $t = 0$). The case of nonzero CEPs is considered in Sec. III C. For convenient reference, the laser parameters for our chirped and unchirped pulses in the $\omega - 2\omega$ and $\omega - 3\omega$ cases are given in Table I.

TABLE I. Laser parameters for the chirped and unchirped pulses used in our HHG calculations. For each component pulse i, we give the carrier wavelength λ_i (nm) ($=2\pi c/\omega_i$), the carrier frequency ω_i (a.u.), the pulse duration τ_i (fs) [see Eq. (11)], the carrier period T_i (fs), and the absolute magnitude of the dimensionless chirp parameter, $|\beta_i|$. For each of the component pulses, the CEP $\phi_i = 0$ and the peak pulse intensity is $I_i = cF_i^2/(8\pi) = 6\times 10^{13}$ W/cm^2.

i	λ_i (nm)	ω_i (a.u.)	τ_i (fs)	T_i (fs)	$\lvert\beta_i\rvert$
1	2400	1.90(−2)	17.9	8.0	2
1	2400	1.90(−2)	17.9	8.0	0
2	1200	3.80(−2)	12.6	4.0	2
2	1200	3.80(−2)	12.6	4.0	0
3	800	5.70(−2)	10.3	2.7	2
3	800	5.70(−2)	10.3	2.7	0

A. Case of ω–2ω chirped laser pulses: HHG enhancement by improving pulse alignment

The $\omega - 2\omega$ fields plotted in Fig. 1 are those for the chirped and unchirped component pulses $i = 1$ and 2 in Table I. The pulse durations of the *unchirped* pulses in Fig. 1(a) are set equal to those of the chirped pulses, i.e., $\Delta_1 = 17.9$ fs and $\Delta_2 = 12.6$ fs with chirp parameters $|\beta_i| = 0$. This is done since the HHG spectrum is sensitive to the pulse length of an ultrashort pulse [22] and our aim here is to isolate the effects of chirp on the HHG spectra.

For the $\omega - 2\omega$ pulse waveform in Fig. 1(a), the peaks of the two component pulses interfere constructively at $t = 0$ where their electric fields are aligned, but interfere destructively at $t = -0.5T_1$ and $+0.5T_1$, at which their electric fields are antialigned. For times approximately a quarter period on either side of $t = \pm 0.5T_1$, the combined field waveform (indicated by the solid line) has two minima. Owing to the periodicity of the $\omega - 2\omega$ fields, if one uses chirp to increase the field minimum in the vicinity of $t = -0.25T_1$, then one expects to also increase the field minimum in the vicinity of $t = +0.75T_1$. These two important minima are highlighted in Fig. 1(a). The increase of the first minimum will increase the ionization rate just before the maximum in the combined field at $t = 0$, while the increase of the second minimum will increase the return energy of electrons ionized by the peak field near $t = 0$. In order to increase the minimum of the $\omega - 2\omega$ waveform near

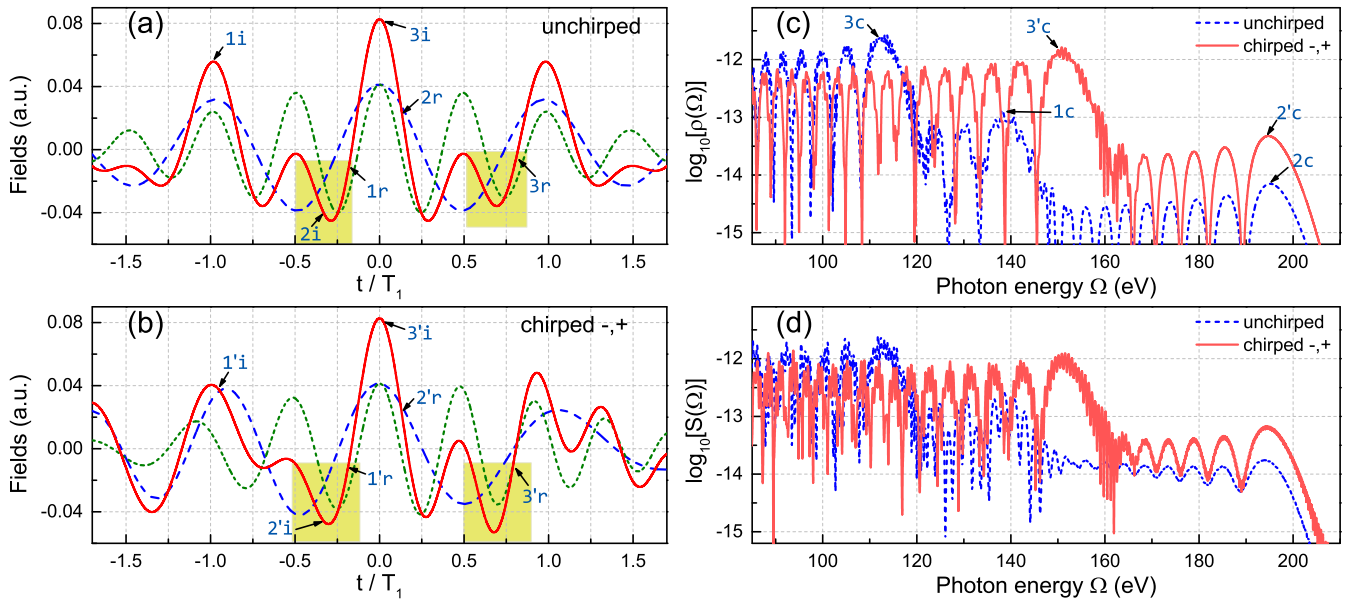

FIG. 1. Two-color ($\omega - 2\omega$) pulse waveforms and their HHG spectra. The ($\omega - 2\omega$) waveforms defined in Eqs. (1) and (8) are composed of component pulse fields $i = 1$ and 2, defined by Eq. (4), having field parameters given in Table I. (a), (b) Electric-field pulses for carrier wavelengths $\lambda_1 = 2400$ nm [long dashed (blue) line], $\lambda_2 = 1200$ nm [short dashed (green) line], and the two-color combined field waveform [solid (red) line] plotted vs time in units of $T_1 \equiv 2\pi/\omega_1 = 8.0$ fs. The arrows indicate the ionization (i) or recombination (r) times of the three electron trajectories given in Table II. Highlighted areas in the vicinity of times $t = -0.25T_1$ and $+0.75T_1$ are discussed in the main text. (c) HHG spectra $\rho(\Omega)$ [see Eq. (16)] produced by the unchirped and chirped pulse waveforms in panels (a) and (b) calculated using the analytic description of short-pulse HHG of Ref. [22]. The arrows indicate the HHG plateau cutoff energies produced by the trajectories listed in Table II. (d) TDSE results $S(\Omega)$ [see Eq. (13)] for the same HHG spectra as in panel (c). To facilitate comparison with the TDSE results $S(\Omega)$ in panel (d), each of the analytic spectra $\rho(\Omega)$ in panel (c) is multiplied by the constant factor 3.08. This factor is chosen so that the values of the TDSE and analytic curves for the unchirped pulses are equal at the position of the lowest cutoff energy, i.e., $\rho(\Omega = 112\ \text{eV}) = S(\Omega = 112\ \text{eV})$ for the unchirped pulses.

$t = -0.25T_1$, one must move the minima of the ω and 2ω component fields at $t = -0.5T_1$ and $-0.25T_1$, respectively, closer together. This can be done by introducing a negative chirp in the ω pulse and a positive chirp in the 2ω pulse. The resultant fields are plotted in Fig. 1(b) and one can see the enhanced field strength in the highlighted areas. Note that the peak intensity of the chirped pulse remains the same as that of the unchirped pulse because the fields are not affected by the chirp at $t = 0$. With this optimization strategy, the HHG spectrum produced by the chirped $\omega - 2\omega$ pulse waveform exhibits a clear enhancement of the HHG yield for harmonic photon energies greater than 120 eV as compared to the HHG spectrum produced by the unchirped $\omega - 2\omega$ pulse waveform, as shown in Figs. 1(c) and 1(d), where we present the HHG spectra produced by our analytic method and by our TDSE method, respectively. We notice also that the cutoff energy of the lower-energy plateau in the HHG spectrum is increased from approximately 112 to 150 eV with only a small decrease in the HHG yield.

In order to determine the physical mechanisms responsible for these enhancements of the HHG spectrum, we employ our analytic description of HHG spectra produced by few-cycle pulses. In this description, the harmonic spectrum is obtained by coherently adding the amplitudes corresponding to a handful of electron trajectories ionized from different half cycles in the vicinity of the maximum of the short-pulse envelope [5]. For each jth electron trajectory, one can calculate the ionization and recombination times $t_i^{(j)}$ and $t_r^{(j)}$, the instantaneous Keldysh parameter $\tilde{\gamma}_j$ at the time of ionization, the ionization factor $\mathcal{I}_j$ (which largely determines the spectral intensity), and the cutoff energy $E_{\text{cut}}^{(j)}$. These quantities are given, respectively, by Eqs. (13), (18), (19), and (25) of Ref. [5] and are listed in Table II for the HHG spectra in Fig. 1(c) produced by the unchirped and chirped $\omega - 2\omega$ pulse waveforms in Figs. 1(a) and 1(b).

TABLE II. Ionization and recombination times $t_i^{(j)}$ and $t_r^{(j)}$ (in units of T_1), cutoff energies $E_{\text{cut}}^{(j)}$, ionization factors $\mathcal{I}_j$, and instantaneous Keldysh parameters $\tilde{\gamma}_j$ for three important electron trajectories j = 1-3 that determine the HHG spectra in Fig. 1(c) produced by the unchirped and chirped $\omega - 2\omega$ pulse waveforms shown in Figs. 1(a) and 1(b).

j	$t_i^{(j)}$	$t_r^{(j)}$	$E_{\text{cut}}^{(j)}$ (eV)	$\mathcal{I}_j$	$\tilde{\gamma}_j$
		(a) Unchirped $\omega - 2\omega$			
1	−0.98	−0.18	138	2.7(−4)	0.68
2	−0.33	0.13	195	5.6(−6)	0.96
3	0.020	0.80	112	3.7(−3)	0.47
		(b) Chirped (−,+)			
1′	−0.96	−0.19	135	4.3(−6)	0.98
2′	−0.33	0.13	194	3.7(−5)	0.83
3′	0.025	0.79	150	3.5(−3)	0.47

In Figs. 1(a) and 1(b) we indicate the ionization and recombination times, $t_i^{(j)}$ and $t_r^{(j)}$, for each of the key electron trajectories j = 1-3 and 1′-3′ given in Table II for the unchirped and chirped $\omega - 2\omega$ pulse waveforms, respectively. Also, in Fig. 1(c) we indicate the cutoff energies for each of these three trajectories for both the unchirped and chirped pulse waveforms.

It is clear from Table II that the approximately order-of-magnitude increase in the HHG yield for harmonic energies greater than 160 eV stems from the nearly order-of-magnitude increase in the ionization rate for electron trajectory $j = 2'$ in the case of the chirped $\omega - 2\omega$ pulse waveform. One sees also that the extension of the lower-energy HHG plateau cutoff energy from 112 to 150 eV is due to the greater recombination energy obtained by the electron on trajectory $j = 3'$, which dominates the spectrum in this energy region. In particular, the significance of the electron trajectory $j = 1'$ is greatly reduced owing to the nearly two-orders-of-magnitude reduction of its ionization rate. Figures 1(c) and 1(d) show also that both the analytic and the TDSE results have fine oscillation structures in the energy region below 160 eV. The origin of these small peaks is the interference of two or more partial amplitudes from different trajectories [22]. For example, for the chirped case in Fig. 1(c), there are three contributing partial amplitudes, 1′, 2′, and 3′. Trajectory 3′ is the dominant one since its ionization factor is more than two orders of magnitude higher than those of the other two, which are responsible for the fine oscillation structures.

The HHG spectra from our analytical calculations in Fig. 1(c) agree well with the TDSE results in Fig. 1(d). The discrepancy in the absolute yields of the analytic and TDSE results by an overall factor is expected, as the analytic theory assumes that the instantaneous Keldysh parameter of the jth trajectory is small, i.e., that $\tilde{\gamma}_j$ is small compared to unity. In the present calculations, this is not always the case (see Table II). The less smooth curves of the TDSE results as compared to the analytic results for harmonic energies above 170 eV may be due to interference of more than one trajectory, whereas the analytic results stem from only the $j = 2$ or $2'$ trajectory in the unchirped and chirped cases, respectively. For clarity, our results in Figs. 1(c) and 1(d) are presented in the high-energy region of the HHG spectrum since it is in this important energy region that chirp effects are most significant.

The optimal combination of chirps for the unchirped $\omega - 2\omega$ pulse waveform in Fig. 1(a) is thus (−,+), in which the ω pulse is negatively chirped and the 2ω pulse is positively chirped. We have also carried out calculations for the other three combinations of chirped pulses: (+,−), (−,−), and (+,+). The resultant HHG spectra are plotted in Fig. 2. In Fig. 2(a) one sees that both the (−,+) and (−,−) chirped pulse waveforms also result in an enhancement of the HHG yield for photon energies above 120 eV, but the optimal (−,+) chirp combination produces the greatest enhancement. In contrast, in Fig. 2(b) one sees that both the (+,−) and (+,+) chirped pulse waveforms result in a decrease in HHG yields as compared to the unchirped pulse case, with the opposite of the optimal combination, i.e., (+,−), giving the lowest HHG yield in the high-energy region. Although Fig. 2 only shows our analytic calculation results for the HHG spectra, results of our TDSE calculations (not shown) are similar.

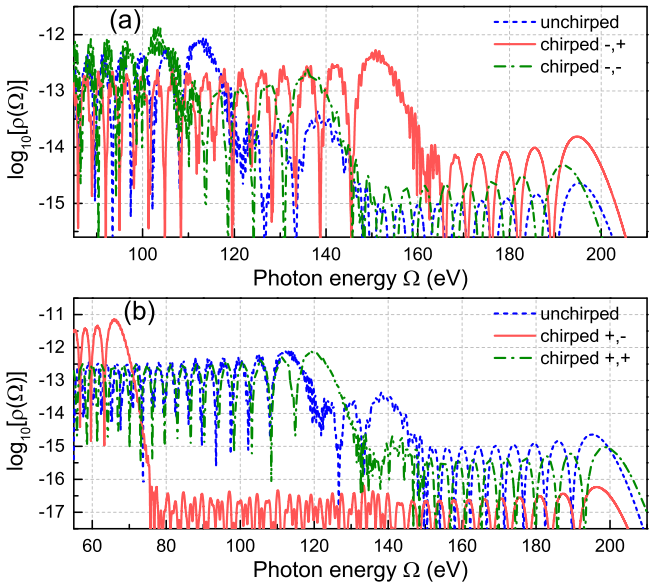

FIG. 2. Comparison of HHG spectra $\rho(\Omega)$ [see Eq. (16)] produced by $\omega - 2\omega$ pulse waveforms with four chirp combinations $\beta = \pm 2$ of the ω and 2ω pulse fields. (a) HHG spectra for the chirp combinations (−,+) and (−,−), where the result for the former is the same as that in Fig. 1(c). (b) HHG spectra for the chirp combinations (+,−) and (+,+). For comparison, in each panel the HHG spectrum produced by the unchirped pulse is also plotted.

B. Case of ω–3ω chirped laser pulses: HHG enhancement by increasing pulse asymmetry

The strategy for enhancing the HHG spectrum produced by an ω–3ω pulse waveform using chirp differs from that for the ω–2ω pulse waveform considered in the previous subsection. In the latter case we have shown that (for pulses with zero CEPs) the ω pulse and 2ω pulse fields are antialigned at $t = \pm 0.5T_1$ [see Fig. 1(a)]. In that case we introduced chirps in the ω pulse and 2ω pulse fields that slightly improved the alignment of the two fields at times $t = \pm 0.5T_1 + 0.25T_1$. In the case of an ω–3ω pulse waveform, however, the ω pulse and 3ω pulse fields are aligned at times $t = \pm 0.5T_1$ and produce nearly symmetric oscillations of the two-color waveform that are centered at times $t = \pm 0.25T_1$ [see highlighted areas in Fig. 3(a)]. In this case the strategy for enhancing HHG yields and increasing HHG plateau cutoff energies is to introduce chirps in the ω pulse and 3ω pulse fields that result in a reduced symmetry of the oscillations centered at $t = \pm 0.25T_1$ in the two-color waveform.

The ω and 3ω pulse fields and their superposition waveform are presented in Fig. 3(a) for the component field parameters given in Table I. Examining the ω–3ω pulse waveform (the solid line) in Fig. 3(a), one sees that electrons ionized by the large field amplitude centered at the time $t = -0.5T_1$ are accelerated back to the atom a half cycle later by the oppositely directed large field amplitude centered at $t = 0$. Similarly, electrons ionized by the large field amplitude centered at $t = 0$ are accelerated back to the atom a half cycle later by the large field amplitude centered at $t = +0.5T_1$. By introducing chirps in the ω pulse and 3ω pulse fields, one can enhance these dominant motions by changing the amplitudes of the

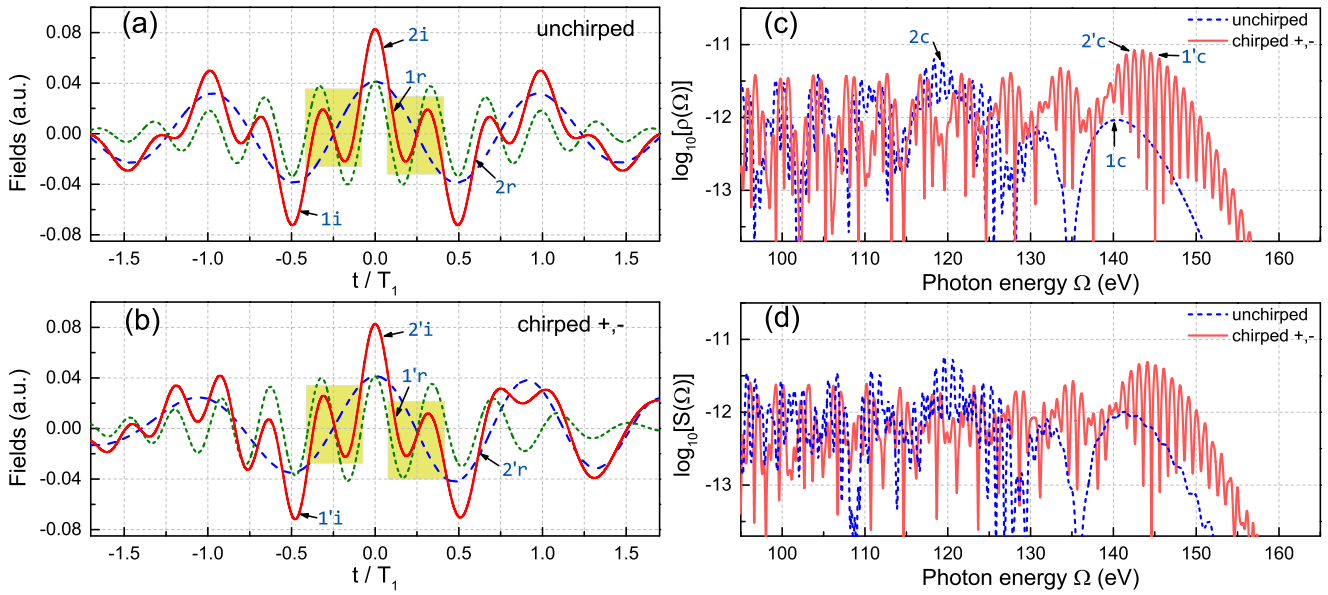

FIG. 3. Two-color ($\omega - 3\omega$) pulse waveforms and their HHG spectra. The ($\omega - 3\omega$) waveforms defined in Eqs. (1) and (9) are composed of component pulse fields $i = 1$ and 3, defined by Eq. (4), having field parameters given in Table I. (a), (b) Electric-field pulses for carrier wavelengths $\lambda_1 = 2400$ nm [long dashed (blue) line], $\lambda_3 = 800$ nm [short dashed (green) line], and the two-color combined field waveform [solid (red) line] plotted vs time in units of $T_1 \equiv 2\pi/\omega_1 = 8.0$ fs. The arrows indicate the ionization (i) or recombination (r) times of two important electron trajectories given in Table III. Highlighted areas in the vicinity of times $t = \pm 0.25T_1$ are discussed in the main text. (c) HHG spectra $\rho(\Omega)$ [see Eq. (16)] produced by the unchirped and chirped pulse waveforms in panels (a) and (b) calculated using the analytic description of short-pulse HHG of Ref. [22]. The arrows indicate the HHG plateau cutoff energies produced by the trajectories listed in Table III. (d) TDSE results $S(\Omega)$ [see Eq. (13)] for the same HHG spectra as in panel (c). To facilitate comparison with the TDSE results $S(\Omega)$ in panel (d), each of the analytic spectra $\rho(\Omega)$ in panel (c) is multiplied by the constant factor 5.81. This factor is chosen so that the values of the TDSE and analytic curves for the unchirped pulses are equal at the position of the lowest cutoff energy, i.e., $\rho(\Omega = 119\ \text{eV}) = S(\Omega = 119\ \text{eV})$ for the unchirped pulses.

small oscillations of the waveform in the highlighted areas in Fig. 3(a) centered at $t = \pm 0.25T_1$. Specifically, one wishes to use chirp to increase the amplitudes of the first half cycles of the oscillations at times $t \lesssim \pm 0.25T_1$ and reduce the amplitudes of the second half cycles of the oscillations at times $t \gtrsim \pm 0.25T_1$. By thus increasing the asymmetry of these two minor half cycles [see the highlighted areas in Fig. 3(a)], the electrons ionized by the peak field amplitudes centered at times $t = -0.5T_1$ and 0 gain more energy during their acceleration back to the atom.

This strategy for using chirp to enhance the HHG spectrum produced by the $\omega - 3\omega$ pulse waveform requires that one positively chirps the ω pulse while negatively chirping the 3ω pulse. As before, our chirp parameter is $|\beta_i| = 2$. By introducing these chirps, the magnitude of the ratio of the amplitude of the first half cycle to the amplitude of the second half cycle in the highlighted area of Fig. 3 at $t = -0.25$ is changed from 0.87 to 1.15. Similarly, the magnitude of the ratio of the amplitude of the first half cycle to the amplitude of the second half cycle in the highlighted area of Fig. 3 at $t = +0.25$ is changed from 1.15 to 1.82. Thus, the $(+,-)$ chirps of the ω and 3ω pulses, respectively, increase the asymmetry in the magnitude of the first half cycle to that of the second half cycle of each of the minor oscillations at times $t = \pm 0.25T_1$. The increase in these asymmetries in turn results in a significant increase of the HHG plateau cutoff energy as well as an increase in the HHG yield above 130 eV, as shown in Figs. 3(c) and 3(d), which present, respectively, our analytic and TDSE results for this ω–3ω case in the high-energy region of the HHG spectrum.

The origin of these enhancements of the HHG spectrum yields and cutoff energies can be understood from our analytic description of short-pulse HHG spectra. For each of the two most important electron trajectories, $j = 1,2$, in the high-energy HHG spectrum, we present in Table III the ionization and recombination times $t_i^{(j)}$ and $t_r^{(j)}$, the instantaneous Keldysh parameter $\tilde{\gamma}_j$ at the time of ionization, the ionization factor $\mathcal{I}_j$ (which largely determines the spectral intensity), and

TABLE III. Ionization and recombination times $t_i^{(j)}$ and $t_r^{(j)}$ (in units of T_1), cutoff energies $E_{\text{cut}}^{(j)}$, ionization factors $\mathcal{I}_j$, and instantaneous Keldysh parameters $\tilde{\gamma}_j$ for two important electron trajectories $j = 1,2$ that determine the high-energy HHG spectra in Fig. 3(c) produced by the unchirped and chirped $\omega - 3\omega$ pulse waveforms shown in Figs. 3(a) and 3(b).

j	$t_i^{(j)}$	$t_r^{(j)}$	$E_{\text{cut}}^{(j)}$ (eV)	$\mathcal{I}_j$	$\tilde{\gamma}_j$
		(a) Unchirped $\omega - 3\omega$			
1	−0.45	0.10	140	1.3(−3)	0.94
2	0.043	0.60	119	3.0(−3)	0.83
		(b) Chirped $(+,-)$			
1′	−0.45	0.11	145	2.6(−3)	0.85
2′	0.035	0.62	142	4.6(−3)	0.78

the cutoff energy $E_{\rm cut}^{(j)}$. In our analytic approach, the amplitudes for these trajectories result in the HHG spectra given in Fig. 3(c) that are produced by the unchirped and chirped $\omega - 3\omega$ pulse waveforms in Figs. 3(a) and 3(b). Comparing the trajectory parameters in Table III for the unchirped and chirped $\omega - 3\omega$ pulse waveforms, one sees that the $j = 2'$ trajectory has a greatly increased cutoff energy as compared to that for the $j = 2$ trajectory. Also, the ionization factors for the $j = 1'$ and $2'$ trajectories are significantly larger than those for the $j = 1$ and 2 trajectories.

In addition to these enhancements, the chirped pulse HHG spectrum has fine-structure oscillations in the energy region above 130 eV that are absent in the unchirped pulse spectrum. These fine-structure oscillations originate from the interference between the two trajectories $j = 1'$ and $2'$ of the chirped pulse. This interference is absent in the unchirped pulse HHG spectrum owing to the very different cutoff energies of the $j = 1$ and 2 trajectories, as shown in Table III. Thus in the energy region from about 135 to 150 eV, the unchirped spectrum is dependent mainly on the $j = 1$ trajectory and hence is quite smooth. By introducing chirps in the ω pulse and 3ω pulse fields, the cutoff energy of the $j = 2'$ trajectory increases from 119 to 142 eV, which is about the same as the cutoff of the $j = 1'$ trajectory. Hence, the fine-structure oscillations with an energy interval of about 1 eV (or about twice the ω photon energy of 0.51 eV) are the result of interference of these two trajectories over the entire high-energy region of the HHG spectrum.

The HHG spectra from our analytical calculations in Fig. 3(c) agree well with the TDSE results in Fig. 3(d). As noted previously, the discrepancy in the absolute yields of the analytic and TDSE results by an overall factor is expected, as the analytic theory assumes that the instantaneous Keldysh parameter of each contributing trajectory is small, i.e., $\tilde{\gamma}_j$ is small compared to unity. In the present calculations, in each case these parameters are smaller than but comparable to unity (see Table II).

The optimal combination of chirps for the unchirped $\omega - 3\omega$ pulse waveform in Fig. 3(a) is thus $(+,-)$, in which the ω pulse is positively chirped and the 3ω pulse is negatively chirped. We have also carried out calculations for the other three combinations of chirped pulses: $(-,-)$, $(-,+)$, and $(+,+)$. The resultant HHG spectra are plotted in Fig. 4. In Fig. 4(a) one sees that both the $(+,-)$ and $(-,-)$ chirped pulse waveforms result in an enhancement of the HHG yield for photon energies above about 130 eV, but the optimal $(+,-)$ chirp combination produces the greatest enhancement, especially above 140 eV. In contrast, in Fig. 4(b) one sees that both the $(-,+)$ and $(+,+)$ chirped pulse waveforms result in a decrease in HHG yields as compared to the unchirped pulse case, with the opposite of the optimal combination, i.e., $(-,+)$, giving the lowest HHG yield in the high-energy region. Although Fig. 4 only shows our analytic calculation results for the HHG spectra, results of our TDSE calculations (not shown) are similar.

C. Cases of ω–2ω and ω–3ω two-color pulses having nonzero CEPs

In Secs. III A and III B we have studied HHG spectra produced by $\omega - 2\omega$ and $\omega - 3\omega$ two-color pulse waveforms and have developed strategies for using chirp to increase HHG yields and plateau cutoff energies. In each of those two cases, the ω pulse and the pulses with carrier frequencies 2ω and 3ω were assumed to have equal peak pulse intensities and zero CEPs. In this section we demonstrate how similar chirp strategies can be used in the case when the CEPs are nonzero. In this case, the ω pulse is no longer aligned with the 2ω or 3ω pulse at $t = 0$. The appropriate strategy is then to use chirps to improve the alignment of the ω pulse field and the field of the 2ω or 3ω pulse at significant times close to $t = 0$. As examples, we consider two cases of two-color pulse waveforms in which the fundamental field has a nonzero CEP ϕ_1. Owing to the generally good qualitative agreement of the results of our analytic description of short-pulse HHG spectra and our TDSE results, in this section we only present results of our analytic description.

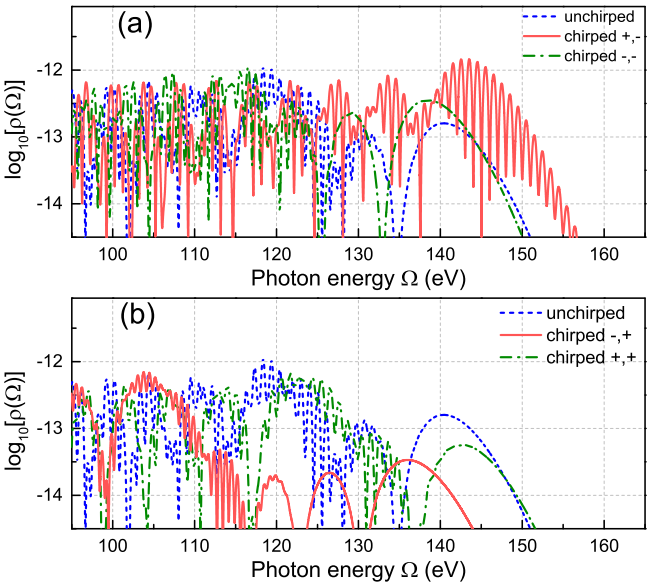

FIG. 4. Comparison of HHG spectra $\rho(\Omega)$ [see Eq. (16)] produced by $\omega - 3\omega$ pulse waveforms with four chirp combinations $\beta = \pm 2$ of the fundamental and harmonic fields. (a) HHG spectra for the chirp combinations $(+,-)$ and $(-,-)$, where the result for the former is the same as that in Fig. 3(c). (b) HHG spectra for the chirp combinations $(-,+)$ and $(+,+)$. For comparison, in each panel the HHG spectrum produced by the unchirped pulse is also plotted.

Consider first the ω–2ω pulse waveform studied in Sec. III A but in which the fundamental field now has a CEP $\phi_1 = \pi/4$. The unchirped ω pulse and 2ω pulse fields as well as the $\omega - 2\omega$ pulse waveform are shown in Fig. 5(a). Examining the highlighted region centered at $t = -0.75T_1$ we see that the ω pulse and 2ω pulse fields both have minima that occur at slightly different times. By introducing chirps, we aim to improve the alignment of these two fields so that the depth of the minimum of the $\omega - 2\omega$ pulse waveform increases. This can be accomplished by introducing a positive chirp $\beta_1 = +2$ in the ω pulse and a negative chirp $\beta_2 = -2$ in the 2ω pulse, as shown in Fig. 5(b). Comparing Figs. 5(a) and 5(b), one sees also that the nearly symmetric oscillation of the two-color pulse waveform centered at about $t = -0.38T_1$ becomes quite asymmetric in the chirped pulse case. The resulting HHG spectra of the chirped and unchirped $\omega - 2\omega$ pulse waveforms are shown

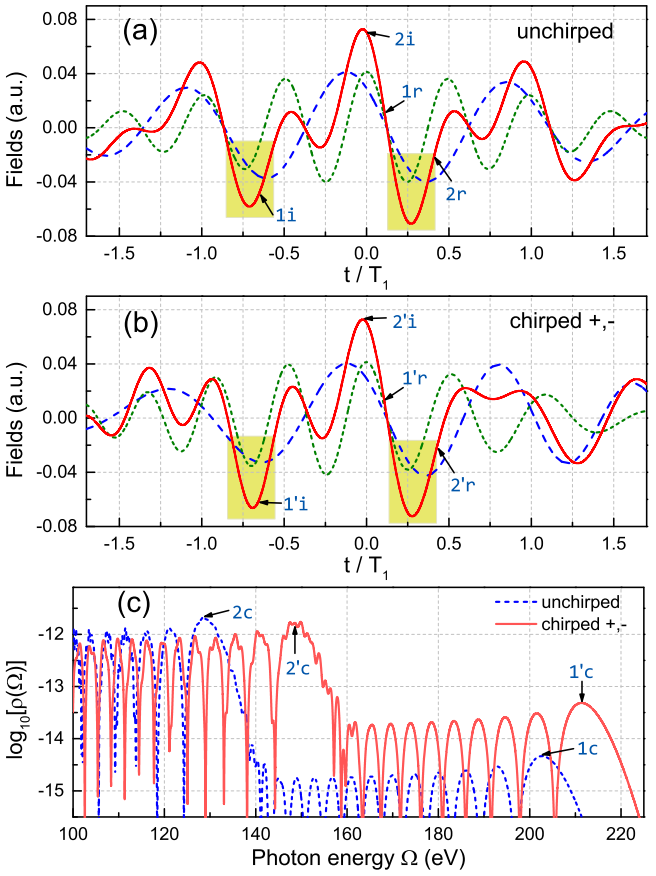

FIG. 5. Two-color ($\omega - 2\omega$) pulse waveforms and their HHG spectra. (a), (b) Electric fields of an ω pulse, a 2ω pulse, and the superposed $\omega - 2\omega$ pulse waveform. The field parameters are the same as in Fig. 1 except that the ω pulse has a nonzero CEP, $\phi_1 = \pi/4$. The arrows indicate the ionization (i) or recombination (r) times given in Table IV for the two most important trajectories. Highlighted areas in the vicinity of times $t = -0.75T_1$ and $+0.25T_1$ are discussed in the main text. (c) HHG spectra $\rho(\Omega)$ [see Eq. (16)] produced by the unchirped and chirped pulse waveforms in panels (a) and (b) calculated using the analytic description of short-pulse HHG of Ref. [22]. The arrows indicate the HHG plateau cutoff energies produced by the trajectories listed in Table IV.

in Fig. 5(c). One observes that the chirped pulse waveform has a much higher HHG yield for harmonic energies above about 135 eV and also that both the low-energy plateau and the high-energy plateau have significantly greater cutoff energies.

Our analytic description of HHG spectra enables us to understand the origin of these enhancements in terms of the two important electron trajectories contributing to the high-energy HHG spectrum. The ionization and recombination times of these two trajectories are indicated in Figs. 5(a) and 5(b) and their respective cutoff energies are indicated in Fig. 5(c). In Table IV we give the values of these parameters of the two trajectories as well as their ionization factors and instantaneous Keldysh parameters. One sees from Fig. 5 and Table IV that the (+,−) chirp has increased the ionization factor for trajectory $j = 1'$ by an order of magnitude, explaining the great increase in yield in the chirped pulse HHG spectrum for harmonic energies greater than about 160 eV. This increase in

TABLE IV. Ionization and recombination times $t_i^{(j)}$ and $t_r^{(j)}$ (in units of T_1), cutoff energies $E_{\rm cut}^{(j)}$, ionization factors $\mathcal{I}_j$, and instantaneous Keldysh parameters $\tilde{\gamma}_j$ for two important electron trajectories $j = 1,2$ that determine the high-energy HHG spectra in Fig. 5(c) produced by the unchirped and chirped $\omega - 2\omega$ pulse waveforms shown in Figs. 5(a) and 5(b).

j	$t_i^{(j)}$	$t_r^{(j)}$	$E_{\rm cut}^{(j)}$ (eV)	$\mathcal{I}_j$	$\tilde{\gamma}_j$
		(a) Unchirped $\omega - 2\omega$			
1	−0.65	0.10	203	5.7(−5)	0.80
2	0.00068	0.41	129	1.6(−3)	0.54
		(b) Chirped (+,−)			
1′	−0.66	0.10	211	6.3(−4)	0.62
2′	−0.0058	0.43	149	1.8(−3)	0.53

the ionization factor of the trajectory $j = 1'$ was accomplished by using chirp to improve the alignment of the minima of the ω pulse and 2ω pulse fields in the highlighted regions in the vicinity of $t = -0.75T_1$ [cf. Figs. 5(a) and 5(b)]. The chirps also increased the alignment of the field minima in the second highlighted regions in Figs. 5(a) and 5(b) near $t = +0.25T_1$. This resulted in an increase in the recombination energy of the trajectory $j = 2'$ by 20 eV, explaining the extension of the low-energy harmonic plateau from 129 to 149 eV. Finally, a small increase in the cutoff energy of the trajectory $j = 1'$ was produced by increasing the asymmetry of the oscillation of the two-color waveform in the vicinity of $t = -0.38T_1$.

Consider second the $\omega - 3\omega$ pulse waveform studied in Sec. III B but in which the ω pulse field now has a nonzero CEP, $\phi_1 = \pi/3$. The unchirped ω pulse and 3ω pulse fields as well as the $\omega - 3\omega$ pulse waveform are shown in Fig. 6(a). Examining the highlighted region located about $t = -0.5T_1$ we see that the ω pulse and 3ω pulse fields both have minima that occur at slightly different times. By introducing chirps, we aim to improve the alignment of these two fields so that the depth of the minimum of the $\omega - 3\omega$ pulse waveform increases. This can be accomplished by introducing a negative chirp $\beta_1 = -2$ in the ω pulse and a positive chirp $\beta_2 = +2$ in the 3ω pulse, as shown in Fig. 6(b). The resulting HHG spectra of the chirped and unchirped $\omega - 3\omega$ pulse waveforms are shown in Fig. 6(c). One observes that the chirped pulse waveform has a much higher HHG yield across the entire harmonic energy spectrum shown.

Our analytic description of HHG spectra enables us to understand the origin of this enhancement of the HHG yield in terms of three important electron trajectories contributing to the high-energy HHG spectrum. The ionization and recombination times of these three trajectories are indicated in Figs. 6(a) and 6(b) and their respective cutoff energies are indicated in Fig. 6(c). In Table V we give the values of these parameters of the three trajectories as well as their ionization factors and instantaneous Keldysh parameters. One sees from Fig. 6 and Table V that the (−,+) chirp has increased the ionization factors significantly for all three trajectories $j = 1',2'$, and $3'$, explaining the great increase in yield in the chirped pulse HHG spectrum for all harmonic energies shown. An increase in the ionization factor of the trajectory $j = 1'$ by nearly three orders of magnitude was accomplished by using chirp to improve

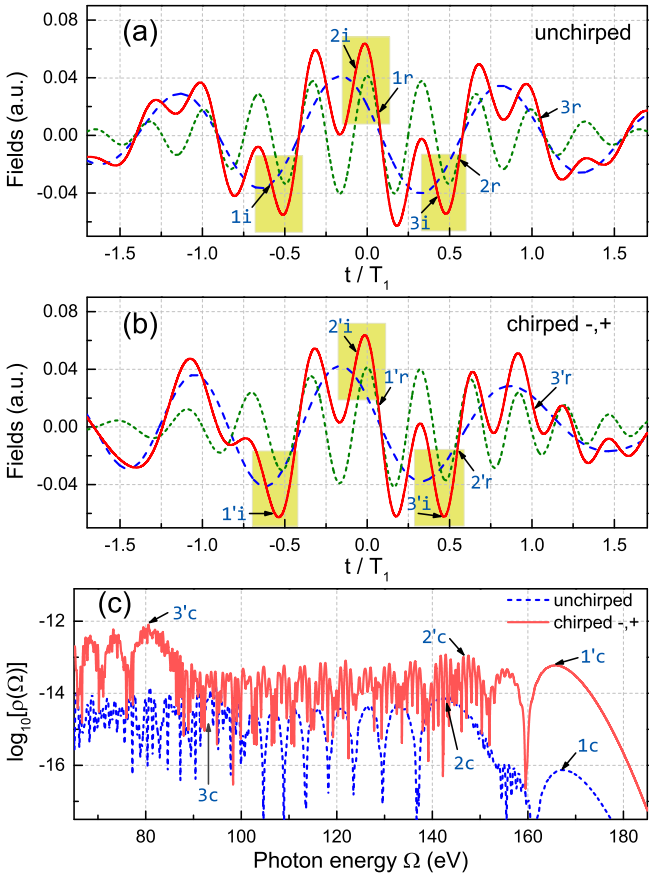

FIG. 6. Two-color ($\omega - 3\omega$) pulse waveforms and their HHG spectra. (a), (b) Electric fields of an ω pulse, a 3ω pulse, and the superposed $\omega - 3\omega$ pulse waveform. The field parameters are the same as in Fig. 3 except that the ω pulse has a nonzero CEP, $\phi_1 = \pi/3$. The arrows indicate the ionization (i) or recombination (r) times given in Table V for the three most important trajectories. Highlighted areas in the vicinity of times $t = \pm 0.5T_1$ are discussed in the main text. (c) HHG spectra $\rho(\Omega)$ [see Eq. (16)] produced by the unchirped and chirped pulse waveforms in panels (a) and (b) calculated using the analytic description of short-pulse HHG of Ref. [22]. The arrows indicate the HHG plateau cutoff energies produced by the trajectories listed in Table V.

TABLE V. Ionization and recombination times $t_i^{(j)}$ and $t_r^{(j)}$ (in units of T_1), cutoff energies $E_{\rm cut}^{(j)}$, ionization factors $\mathcal{I}_j$, and instantaneous Keldysh parameters $\tilde{\gamma}_j$ for three important electron trajectories $j = 1,2,3$ that determine the high-energy HHG spectra in Fig. 6(c) produced by the unchirped and chirped $\omega - 3\omega$ pulse waveforms shown in Figs. 6(a) and 6(b).

j	$t_i^{(j)}$	$t_r^{(j)}$	$E_{\rm cut}^{(j)}$ (eV)	$\mathcal{I}_j$	$\tilde{\gamma}_j$
			(a) Unchirped $\omega - 3\omega$		
1	−0.58	0.068	167	1.2(−6)	1.7
2	−0.067	0.56	142	8.5(−5)	1.2
3	0.43	1.1	93.1	3.2(−5)	1.3
			(b) Chirped (−,+)		
1′	−0.57	0.067	166	9.5(−4)	0.97
2′	−0.059	0.55	146	2.4(−4)	1.1
3′	0.46	1.0	80.6	1.5(−3)	0.92

the alignment of the minima of the ω pulse and the 3ω pulse fields in the highlighted regions in the vicinity of $t = -0.5T_1$ [cf. Figs. 6(a) and 6(b)]. The chirps also increased the alignment of the field minima in the third highlighted regions in Figs. 6(a) and 6(b) near $t = +0.5T_1$. This resulted in an increase in the ionization factor of the trajectory $j = 3'$ by nearly two orders of magnitude, explaining the increase in the yield of the low-energy HHG plateau (at the cost of a slightly lower cutoff energy). Finally, a small increase in the ionization factor of the trajectory $j = 2'$ was produced by improving the alignment of the fundamental and third harmonic fields in the second highlighted region located near $t = 0$. This increase in the ionization factor of the $j = 2'$ trajectory contributed to the increase in the HHG yield for harmonic energies from about 90 to 150 eV.

D. Applicability to other atoms

Although our analysis of chirp effects in a two-color field has been presented for a one-electron system, the results we obtain should be applicable also for many-electron systems. Specifically, in this paper we have presented results for the H atom because electron correlation effects are absent and hence our TDSE results are exact. In the three-step analytic model for HHG that we have employed, the first step depends only on the binding energy of the valence electron. Since Ar and many other atoms have binding energies comparable (within a few eV) to that for the H atom and since the second step of the three-step model treats the electron as moving freely in the laser field, these two steps are similar for a wide range of atoms. The main atom-specific part of the three-step model is the recombination step. For the H atom, this third step is known analytically and for other atoms the third (recombination) step can be obtained from existing fully correlated results for photoionization cross sections (using the principle of detailed balance).

The factorization of the HHG spectrum into a quasiuniversal "electron wave packet" factor (produced by the first two steps of the three-step model) and a target-specific recombination factor has been successfully employed to describe HHG by atoms [34–37] as well as by ions [38] and molecules [39]. Whereas the H atom photoionization cross section is smoothly decreasing, those for rare gas atoms can have structure, which is reflected in the HHG spectra, as has been confirmed experimentally [40]. However, all of the results we present in the current paper have mainly to do with the first two steps of the three-step model, i.e., the ionization and the excursion of the active electron away from and back to the ion. Whatever the recombination amplitude happens to be for other atomic, ionic, or molecular targets, the HHG yield will increase if the active electron moves under the influence of the chirped fields we propose. In brief, since the chirp effects on HHG spectra that we present originate from laser-induced electron dynamics, which have been shown to be independent of electron correlation effects in numerous prior studies [34–40], they are expected to be applicable to any atomic (or molecular) system.

IV. SUMMARY AND CONCLUSIONS

We have studied how chirp can be used to enhance the yields and plateau cutoff energies of the HHG spectrum produced

by a few-cycle, linearly polarized pulse waveform composed of two-color component pulses that are linearly chirped. We have studied two common two-color cases: $\omega - 2\omega$ pulses and $\omega - 3\omega$ pulses, in which either the ω pulse and the 2ω or 3ω pulses have zero CEPs or in which the ω pulse has a nonzero CEP. In all cases we consider only chirp parameters having the same magnitude, so that our focus is on the signs of the chirps in the ω pulse and the 2ω or 3ω pulses. As we have shown, the general strategy is twofold. In cases in which major peaks of the two-color component pulses are not aligned, one can use the chirp to improve the alignment by bringing the neighboring minima or maxima closer to each other in time, so that the resultant field has a higher strength and consequently leads to an increased yield of the HHG spectrum. In cases in which the major peaks of the two-color fields are aligned, chirps can be used to enhance the asymmetry of smaller peaks so that the net acceleration of the ionized electron back to the atom leads to an increased recombination energy and, hence, a higher HHG plateau cutoff energy. In both cases, one should positively chirp one color and negatively chirp the other in order to achieve the best enhancement of the HHG spectrum. The physical mechanisms responsible for these enhancements can be explained based on the well-known three-step model of HHG [1,23–26].

To conclude, two things should be noted. First, our studies have focused on the use of chirp to sculpt two-color pulse waveforms in order to enhance HHG spectra based on a semiclassical analytic analysis of the unchirped waveforms. This analytic approach to optimal control of HHG differs from approaches based upon various kinds of iterative algorithms, although both approaches share the same goals. Second, for all cases we consider, enhanced HHG spectra result from oppositely chirping the two-color pulses, i.e., the ω pulse and the 2ω– or 3ω pulse should be chirped either in the combination of $(+,-)$ or $(-,+)$. Experiments can thus try these two possible chirp strategies to see which works best in enhancing the HHG spectrum as compared to that obtained using unchirped two-color pulses. Thus this paper contributes to a more comprehensive understanding of how to sculpt synthesized waveforms of two-color, few-cycle pulses, which can benefit not only HHG but also attosecond pulse generation and other related topics.

ACKNOWLEDGMENTS

This paper was supported in part by NSF Grant No. PHYS-1505492. Our TDSE calculations were completed utilizing the Holland Computing Center of the University of Nebraska, Lincoln (UNL), which receives support from the Nebraska Research Initiative. Collaborative visits to UNL by M.V.F. were supported in part by NSF EPSCoR IRR Track II Research Award No. 1430519. The research of M.V.F. is supported in part by the Russian Science Foundation through Grant No. 18-12-00476 and by the Ministry of Education and Science of the Russian Federation through Grant No. 3.1659.2017/4.6.

[1] F. Krausz and M. Ivanov, Attosecond physics, Rev. Mod. Phys. **81**, 163 (2009).

[2] A. de Bohan, Ph. Antoine, D. B. Milošević, and B. Piraux, Phase-Dependent Harmonic Emission with Ultrashort Laser Pulses, Phys. Rev. Lett. **81**, 1837 (1998).

[3] J. J. Carrera and S.-I. Chu, Extension of high-order harmonic generation cutoff via coherent control of intense few-cycle chirped laser pulses, Phys. Rev. A **75**, 033807 (2007).

[4] M. Lara-Astiaso, R. E. F. Silva, A. Gubaydullin, P. Rivière, C. Meier, and F. Martín, Enhancing High-Order Harmonic Generation in Light Molecules by Using Chirped Pulses, Phys. Rev. Lett. **117**, 093003 (2016).

[5] D. Peng, L.-W. Pi, M. V. Frolov, and A. F. Starace, Enhancing high-order-harmonic generation by time delays between two-color, few-cycle pulses, Phys. Rev. A **95**, 033413 (2017).

[6] R. Bartels, S. Backus, E. Zeek, L. Misoguti, G. Vdovin, I. P. Christov, M. M. Murnane, and H. C. Kapteyn, Shaped-pulse optimization of coherent emission of high-harmonic soft X-rays, Nature (London) **406**, 164 (2000).

[7] P. Wei, J. Miao, Z. Zeng, C. Li, X. Ge, R. Li, and Z. Xu, Selective Enhancement of a Single Harmonic Emission in a Driving Laser Field with Subcycle Waveform Control, Phys. Rev. Lett. **110**, 233903 (2013).

[8] X. Wang, C. Jin, and C. D. Lin, Coherent control of high-harmonic generation using waveform-synthesized chirped laser fields, Phys. Rev. A **90**, 023416 (2014).

[9] L. E. Chipperfield, J. S. Robinson, J. W. G. Tisch, and J. P. Marangos, Ideal Waveform to Generate the Maximum Possible Electron Recollision Energy for Any Given Oscillation Period, Phys. Rev. Lett. **102**, 063003 (2009).

[10] I.-L. Liu, P.-C. Li, and S.-I. Chu, Coherent control of the electron quantum paths for the generation of single ultrashort attosecond laser pulse, Phys. Rev. A **84**, 033414 (2011).

[11] S. Haessler, T. Balčiunas, G. Fan, G. Andriukaitis, A. Pugžlys, A. Baltuška, T. Witting, R. Squibb, A. Zaïr, J. W. G. Tisch, J. P. Marangos, and L. E. Chipperfield, Optimization of Quantum Trajectories Driven by Strong-Field Waveforms, Phys. Rev. X **4**, 021028 (2014).

[12] C. Jin, G. Wang, H. Wei, A.-T. Le, and C. D. Lin, Waveforms for optimal sub-keV high-order harmonics with synthesized two- or three-colour laser fields, Nat. Commun. **5**, 4003 (2014).

[13] J. Solanpää, J. A. Budagosky, N. I. Shvetsov-Shilovski, A. Castro, A. Rubio, and E. Räsänen, Optimal control of high-harmonic generation by intense few-cycle pulses, Phys. Rev. A **90**, 053402 (2014).

[14] Y. Chou, P.-C. Li, T.-S. Ho, and S.-I. Chu, Optimal control of high-order harmonics for the generation of an isolated ultrashort attosecond pulse with two-color midinfrared laser fields, Phys. Rev. A **91**, 063408 (2015).

[15] C. Jin, G. J. Stein, K.-H. Hong, and C. D. Lin, Generation of Bright, Spatially Coherent Soft X-Ray High Harmonics in a Hollow Waveguide Using Two-Color Synthesized Laser Pulses, Phys. Rev. Lett. **115**, 043901 (2015).

[16] M. R. Edwards and J. M. Mikhailova, Waveform-Controlled Relativistic High-Order-Harmonic Generation, Phys. Rev. Lett. **117**, 125001 (2016).

[17] C. Manzoni, O. D. Mücke, G. Cirmi, S. Fang, J. Moses, S.-W. Huang, K.-H. Hong, G. Cerullo, and F. X. Kärtner, Coherent pulse synthesis: towards sub-cycle optical waveforms, Laser Photon. Rev. **9**, 129 (2015).

[18] Z. Chang, A. Rundquist, H. Wang, I. Christov, H. C. Kapteyn, and M. M. Murnane, Temporal phase control of soft-x-ray harmonic emission, Phys. Rev. A **58**, R30 (1998).

[19] P. Salières, Ph. Antoine, A. de Bohan, and M. Lewenstein, Temporal and Spectral Tailoring of High-Order Harmonics, Phys. Rev. Lett. **81**, 5544 (1998).

[20] D. G. Lee, J.-H. Kim, K.-H. Hong, and C. H. Nam, Coherent Control of High-Order Harmonics with Chirped Femtosecond Laser Pulses, Phys. Rev. Lett. **87**, 243902 (2001).

[21] M. Murakami, J. Mauritsson, and M. B. Gaarde, Frequency-chirp rates of harmonics driven by a few-cycle pulse, Phys. Rev. A **72**, 023413 (2005).

[22] M. V. Frolov, N. L. Manakov, A. M. Popov, O. V. Tikhonova, E. A. Volkova, A. A. Silaev, N. V. Vvedenskii, and A. F. Starace, Analytic theory of high-order-harmonic generation by an intense few-cycle laser pulse, Phys. Rev. A **85**, 033416 (2012).

[23] K. J. Schafer, B. Yang, L. F. DiMauro, and K. C. Kulander, Above Threshold Ionization beyond the High Harmonic Cutoff, Phys. Rev. Lett. **70**, 1599 (1993).

[24] P. B. Corkum, Plasma Perspective on Strong Field Multiphoton Ionization, Phys. Rev. Lett. **71**, 1994 (1993).

[25] K. C. Kulander, K. J. Schafer, and J. L. Krause, Dynamics of Short-Pulse Excitation, Ionization and Harmonic Conversion, in *Super-Intense Laser-Atom Physics*, edited by B. Piraux, A. L'Huillier, and K. Rzążewski (Plenum, New York, 1993), pp. 95–110.

[26] M. Lewenstein, Ph. Balcou, M. Yu. Ivanov, A. L'Huillier, and P. B. Corkum, Theory of high-harmonic generation by low-frequency laser fields, Phys. Rev. A **49**, 2117 (1994).

[27] G. L. Yudin, A. D. Bandrauk, and P. B. Corkum, Chirped Attosecond Photoelectron Spectroscopy, Phys. Rev. Lett. **96**, 063002 (2006).

[28] L.-Y. Peng, F. Tan, Q. Gong, E. A. Pronin, and A. F. Starace, Few-cycle attosecond pulse chirp effects on asymmetries in ionized electron momentum distributions, Phys. Rev. A **80**, 013407 (2009).

[29] E. J. Takahashi, P. Lan, O. D. Mücke, Y. Nabekawa, and K. Midorikawa, Infrared Two-Color Multicycle Laser Field Synthesis for Generating an Intense Attosecond Pulse, Phys. Rev. Lett. **104**, 233901 (2010).

[30] S.-W. Huang, G. Cirmi, J. Moses, K.-H. Hong, S. Bhardwaj, J. R. Birge, L.-J. Chen, E. Li, B. J. Eggleton, G. Cerullo, and F. X. Kärtner, High-energy pulse synthesis with sub-cycle waveform control for strong-field physics, Nature Photonics **5**, 475 (2011).

[31] A Wirth, M. Th. Hassan, I. Grguraš, J. Gagnon, A. Moulet, T. T. Luu, S. Pabst, R. Santra, Z. A. Alahmed, A. M. Azzeer, V. S. Yakovlev, V. Pervak, F. Krausz, and E. Goulielmakis, Synthesized Light Transients, Science **334**, 195 (2011).

[32] X.-M. Tong and S.-I. Chu, Theoretical study of multiple high-order harmonic generation by intense ultrashort pulsed laser fields: A new generalized pseudospectral time-dependent method, Chem. Phys. **217**, 119 (1997).

[33] A. D. Bandrauk, S. Chelkowski, D. J. Diestler, J. Manz, and K.-J. Yuan, Quantum simulation of high-order harmonic spectra of the hydrogen atom, Phys. Rev. A **79**, 023403 (2009).

[34] T. Morishita, A.-T. Le, Z. Chen, and C. D. Lin, Accurate Retrieval of Structural Information from Laser-Induced Photoelectron and High-Order Harmonic Spectra by Few-Cycle Laser Pulses, Phys. Rev. Lett. **100**, 013903 (2008).

[35] A.-T. Le, T. Morishita, and C. D. Lin, Extraction of the species-dependent dipole amplitude and phase from high-order harmonic spectra in rare-gas atoms, Phys. Rev. A **78**, 023814 (2008).

[36] M. V. Frolov, N. L. Manakov, T. S. Sarantseva, M. Yu. Emelin, M. Yu. Ryabikin, and A. F. Starace, Analytic Description of the High-Energy Plateau in Harmonic Generation by Atoms: Can the Harmonic Power Increase with Increasing Laser Wavelengths? Phys. Rev. Lett. **102**, 243901 (2009).

[37] M. V. Frolov, N. L. Manakov, A. A. Silaev, N. V. Vvedenskii, and A. F. Starace, High-order harmonic generation by atoms in a few-cycle laser pulse: Carrier-envelope phase and many-electron effects, Phys. Rev. A **83**, 021405(R) (2011).

[38] M. V. Frolov, N. L. Manakov, and A. F. Starace, Potential barrier effects in high-order harmonic generation by transition-metal ions, Phys. Rev. A **82**, 023424 (2010).

[39] A.-T. Le, R. R. Lucchese, S. Tonzani, T. Morishita, and C. D. Lin, Quantitative rescattering theory for high-order harmonic generation from molecules, Phys. Rev. A **80**, 013401 (2009).

[40] A. D. Shiner, B. E. Schmidt, C. Trallero-Herrero, H. J. Wörner, S. Patchkovskii, P. B. Corkum, J-C. Kieffer, F. Légaré, and D. M. Villeneuve, Probing collective multi-electron dynamics in xenon with high-harmonic spectroscopy, Nat. Phys. **7**, 464 (2011).